Seed-Mediated Growth of Ag@Au Nanodisks with Improved Chemical Stability and Surface-Enhanced Raman Scattering

Siva Kumar Krishnan,[*,†] Rodrigo Esparza,[‡] F. J. Flores-Ruiz,[†] Erika Padilla-Ortega,[§] Gabriel Luna-Bárcenas,[∥] Isaac. C. Sanchez,[⊥] and Umapada Pal[#]

[†]CONACYT-Instituto de Física and [#]Instituto de Física, Benemérita Universidad Autónoma de Puebla, Apdo. Postal J-48, Puebla 72570, Mexico

[‡]Centro de Física Aplicada y Tecnología Avanzada, Universidad Nacional Autónoma de México, Boulevard Juriquilla 3001, Santiago de Querétaro, Querétaro 76230, Mexico

[§]Graduate Multidisciplinary Program in Environmental Sciences, Autonomous University of San Luis Potosi, San Luis Potosi 78210, Mexico

[∥]Cinvestav Querétaro, Querétaro, Querétaro 76230, Mexico

[⊥]Department of Chemical Engineering, The University of Texas at Austin, Austin, Texas 78712, United States

ⓢ *Supporting Information*

ABSTRACT: Bimetallic Ag@Au nanoparticles (NPs) have received significant research interest because of their unique optical properties and molecular sensing ability through surface-enhanced Raman scattering (SERS). However, the synthesis of Ag@Au core−shell plasmonic nanostructures with precisely controlled size and shape remained a great challenge. Here, we report a simple approach for the synthesis of bimetallic Ag@Au nanodisks of about 13.5 nm thickness and different diameters through a seed-mediated growth process. The synthesis involves the conformal deposition of Au atoms at the corner sites of Ag nanoplate (AgNPL) seeds coupled with site-selective oxidative etching of AgNPL edges to generate Ag@Au nanodisks. The resultant Ag@Au nanodisks manifest significantly improved chemical stability and tunable localized surface plasmon resonance from the visible to the near-infrared spectral range. Moreover, in comparison to AgNPLs, the Ag@Au nanodisks

showed greatly enhanced SERS performance with an enhancement factor up to 0.47×10^5, which is nearly 3-fold higher than that of the original AgNPLs (0.18×10^5). Furthermore, the Ag@Au nanodisks show a high sensitivity for detecting probe molecules such as crystal violet of concentration as low as 10^{-9} M and excellent reproducibility, with the SERS intensity fluctuation less than 12.5%. The synthesis route adapted for the controlled fabrication of Ag@Au nanodisks can be a potential platform for maneuvering other bimetallic plasmonic nanostructures useful for plasmonics and sensing applications.
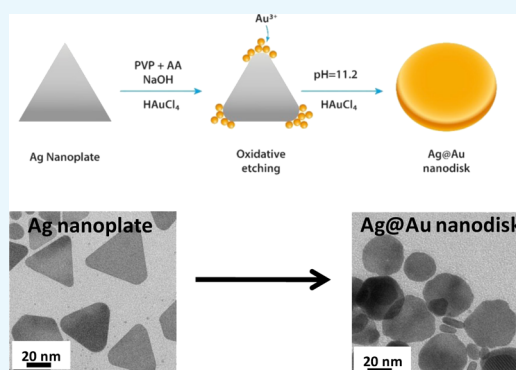
■ INTRODUCTION

Noble metal nanostructures have generated a huge research interest owing to their unique tunable localized surface plasmon resonance (LSPR) properties,[1] which render their widespread application in various fields such as photocatalysis,[2] plasmonics,[3,4] surface-enhanced Raman scattering (SERS),[5] biosensing,[6] and biomedicine.[7] Since its discovery, SERS has been regarded as a fascinating analytical technique for detecting analyte molecules with ultrahigh sensitivity.[8−10] Noble metal nanoparticles (NPs) such as Ag[3,11,12] and Au[13−16] with various shapes have been widely investigated for SERS applications because of their morphology-dependent high anisotropy and tunable LSPR, which can produce strong electromagnetic (EM) fields localized around the NP surface, resulting in the generation of near-field enhancement effects.[17] In particular, triangular Ag nanoplates (NPLs) with relatively larger {111} facets have been found to exhibit a strong coupling of LSPR with

the analyte molecules because of the strong EM field accumulation at their edges,[18] manifesting a highly enhanced SERS signal for a variety of analyte molecules.[16] However, the Ag NPLs are thermodynamically unstable, and the poor chemical stability toward oxidation in physiological conditions is the principal limitation for their use in practical applications.[19] On the other hand, Ag@Au core−shell-type bimetallic NPs have received considerable attention because of their improved chemical stability and the possibility of tuning the LSPR peak positions from the visible to the near-infrared (NIR) region by tailoring their structure and composition.[20−26] Intensive research efforts have been made on controlling the LSPR properties and the enhancement of chemical stability of such

core–shell-type bimetallic nanostructures.[11,27−30] Specifically, the controlled growth of an ultrathin Au shell around Ag seeds to obtain bimetallic Ag@Au core–shell structures is largely considered to be a promising strategy to tune the LSPR and enhance the chemical stability of the plasmonic nanostructure.[27,29] As an example, Yang et al.[28] showed that the conformal deposition of an Au shell of a few atomic-layer thickness (6 atomic layers of Au) over Ag nanocubes can significantly improve their chemical stability and SERS activity.

Recently, seed-mediated solution-phase growth process has become the most attractive technique for the preparation of nanocrystals of bimetallic/multimetallic systems with well-controlled size and shape.[31,32] The controlled synthesis of Ag@Au NPs of diverse shapes with a finely tuned LSPR peak position from the visible to the IR region has been extensively reported in the literature.[29,30,32−34] However, the fabrication of bimetallic Ag@Au core–shell NPs with spatial control over the shell thicknesses remained a great challenge. This challenge primarily arises because of the inherent galvanic exchange reaction that occurred between the Ag NP seeds and Au^{3+}, making the uniform deposition of Au over Ag NPs extremely difficult, which usually leads to the formation of hollow nanoframes.[35−37] Considerable efforts have been made to overcome this obstacle by preventing the galvanic reaction, achieving an Au shell of varying thickness onto the Ag NP seeds.[38−40] Yang et al.[28] developed a strategy for the synthesis of Ag@Au core–shell nanocubes with 3–6 atomic layers of Au-shell thickness by the parallel reduction of Au^{3+} atoms onto the cubic Ag seeds using ascorbic acid (AA), where the reduction of Au^{3+} ion dominated by AA resulted in the suppression of the galvanic reaction between Ag and Au^{3+}.[28] Recently, Cathcart et al.[30] demonstrated an effective deposition of Au onto the Ag NP seeds assisted by poly(styrenesulfonate) to obtain Ag@Au core–shell NPs with tunable LSPR from 470 to 800 nm, with a greatly improved chemical stability. On the other hand, oxidative etching of metal NPs has been extensively reported as a novel strategy to control the shape of the metal NPs.[41] For instance, Hong et al.[42] described a process of oxidative etching of Au NPLs by the chlorine ions of the Au precursor, capable of producing Au NPs of different shapes. Lin et al.[43] reported a facile synthesis process for the fabrication of uniform spherical Ag NPs via the seed-mediated growth coupled with oxidative etching of Ag nanocubes using Cu^{2+} ions. Despite all these efforts, the process of controlled synthesis of Ag@Au core–shell nanostructures with desired sizes and shapes remained unclear.

Herein, we present a facile, seed-mediated strategy for the fabrication of Ag@Au nanodisks through a galvanic reaction-free deposition of Au atoms onto Ag NPLs followed by tip-selective oxidative etching reactions. The galvanic etching-free deposition of Au atoms and oxidative etching occur simultaneously after the injection of $HAuCl_4$ at a relatively higher reaction pH, which leads to a shape evolution from AgNPLs to Ag@Au nanodisks. The resultant Ag@Au nanodisks exhibit excellent chemical stability, and their LSPR peak position can be tuned from 656 to 780 nm just by varying their diameter. Furthermore, owing to the unique disk-like structure of the Ag@Au nanodisks and their LSPR position matching with the laser excitation wavelength (785 nm), the nanostructures manifest significantly improved SERS performance for the detection of crystal violet (CV) molecules with a concentration as low as 10^{-9} M.

RESULTS AND DISCUSSION

Synthesis and Characterization of Ag@Au Nanodisks. The triangular Ag NPLs of 20−35 nm edge lengths (Figure S1) were synthesized following the procedure reported previously.[44] The bimetallic Ag@Au core–shell nanodisks were obtained by the deposition of reduced Au atoms onto the triangular Ag NPL seeds and further controlled oxidative dissolutions at the tips using polyvinylpyrrolidone (PVP) as the surfactant and AA as the reducing agent. The pH value of the reaction solution was adjusted to 11.2 by adding NaOH (0.2 M) solution, with a subsequent addition of the $HAuCl_4$ precursor solution at a relatively slow injection rate. Recent studies have shown that the introduction of $HAuCl_4$ solution at a higher pH (pH = 11.2) reduces the reduction potential of gold ions significantly, which enables the conformal deposition of uniform metallic shells over the Ag seeds.[45] Specifically, during the slow titration in the presence of NaOH, after the quick neutralization of $HAuCl_4$ by OH^-, the produced $[AuCl_4]^-$ undergo a ligand exchange process with OH^- to generate $AuCl(OH)_3^-$ and $Au(OH)_4^-$, which have a lower reduction potential than the $[AuCl_4]^-$.[46] By controlling the degree of the neutralization process, the smoothness of Au shells and the morphology of the resultant Ag@Au NPs could be effectively tailored by avoiding the galvanic reaction.[47] On the other hand, the presence of Cl^- ions generated from the dissociation of $AuCl_4$ favors the selective oxidative etching of the edges of the Ag NPLs.[48,49]

The growth of bimetallic Ag@Au nanodisks reported here is distinct from the previous studies as we combine both the galvanic reaction-free deposition of Au and oxidative dissolution reaction of the edges of Ag NPLs to obtain Ag@Au core–shell nanodisks. The suppression of galvanic replacement at room temperature was demonstrated by Yang et al. for Ag@Au nanocubes,[28] and the strategy has been extended by several other groups for the fabrication of other bimetallic systems.[29,50] On the other hand, the oxidative dissolution reaction has been exploited to other NP systems for controlled transformation of their shapes into other morphologies.[12,41,42,51,52] As an example, O'Brien et al.[52] have demonstrated the transformation of hexagonal Au NPLs to uniform Au circular disks through selective oxidative etching in the presence of cetyltrimethylammonium bromide (CTAB). Uniform circular Au nanodisks were obtained because of the strong binding of $HAuCl_4$ with CTAB, which enabled the reaction to proceed with the lowest metal coordination number in a self-limiting fashion, followed by selective oxidation at the tip of the Au NPLs by Au^{3+} ions. In the present synthesis, as the selective oxidation of the tip edges of triangular Ag NPLs was performed without a strong reducing agent, the galvanic replacement reaction is unavoidable, which usually leads to the formation of bimetallic nanoframes.[36] The key premise of this synthesis is that the slow addition of $HAuCl_4$ at a higher pH (pH = 11.2) by introducing aqueous NaOH solution decreases the reduction potential of $[AuCl_4]^-$. Consequently, a conformal deposition of reduced Au atoms occurs onto Ag NPLs by avoiding the galvanic reaction, and further a conproportionation reaction occurs selectively at the corner sites of the Ag NPLs rather than the other faces. By increasing the amount of $HAuCl_4$, the Ag NPLs could be converted into Ag@Au core–shell nanodisks through the oxidative dissolution reaction.

A schematic illustration of the steps involved in the controlled transformation from the triangular Ag NPLs into Ag@Au nanodisks is presented in Figure 1A. To understand the
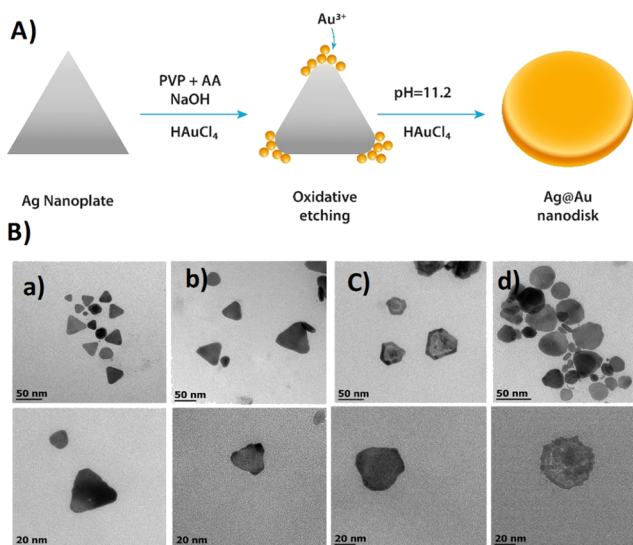
Figure 1. (A) Schematic representation of the formation of Ag@Au nanodisks from Ag NPL seeds as a function of HAuCl$_4$ concentration; (B) corresponding TEM images showing (a) Ag NPLs and (b−d) evolution of Ag@Au nanodisks at different growth stages upon increasing the amount of HAuCl$_4$ confirming the tip-selective oxidative dissolution at the tips of Ag NPLs and conformal deposition.

synthetic steps better, we carried out the transmission electron microscopy (TEM) analysis of the samples prepared at different Au precursor concentrations (Figure 1B). The TEM results in Figure 1B(a−d), confirm the reduced Au atoms are selectively bonded at the tips of the Ag NPLs instead of other triangular faces. For Au precursor concentrations higher than the optimum, the reduced Au atoms diffuse to the triangular faces, and oxidative dissolution takes place at the edges of the Ag NPLs to gradually evolve into circular disk-like structures. It is evident that the galvanic replacement-free conformal deposition of Au atoms proceeds selectively at the tips of the Ag NPLs, which serve as initial seeding sites for controlled oxidation at the edges and subsequent diffusion of Au atoms to other faces.[52]

Figure 2a−d shows the low- and high-magnification TEM images of the triangular Ag NPL seeds and the obtained bimetallic Ag@Au nanodisks. The formation of triangular Ag NPLs with sharp corners along with a few hexagonal particles is evident in the TEM images presented in Figure 2a,b. Figure 2c,d displays the TEM images of Ag@Au nanodisks after their transformation from Ag NPLs. The formation of uniform disk-like structures with an average size of ca. 45 nm is very clear from these micrographs. The distribution of the elements (Au and Ag) in the disk-like final structures can be seen in the energy-dispersive spectrometry (EDS) elemental mapping images presented in Figures 2e−g. The elemental mapping images clearly demonstrate that Ag (green) is located at the core and Au (red) remains around the Ag core in the Ag@Au nanodisks. Furthermore, we carried out atomic force microscopy (AFM) imaging of the Ag NPLs and Ag@Au nanodisks to estimate their thicknesses. Typical topographic images of Ag NPLs and Ag@Au nanodisks and their height profiles are displayed in Figure 3. The AFM images confirm the formation of Ag NPLs (Figure 3a,b) and Ag@Au nanodisks (Figure 3d,e). The surface height profile plots (Figure 3c,f) further reveled the smooth non-corrugated surface of the bimetallic nanodisks. The thicknesses of the Ag NPLs and Ag@Au nanodisks were determined to be 10 and 13.5 nm, respectively.
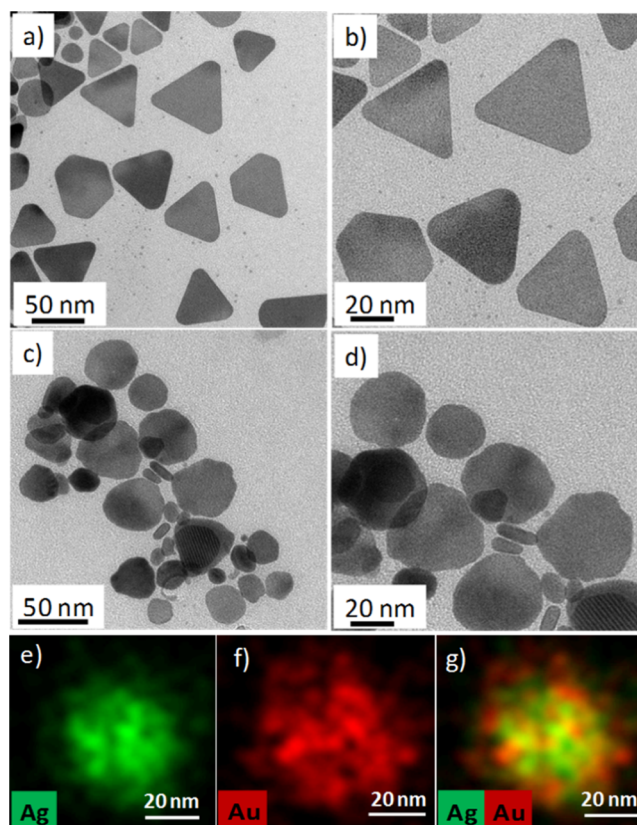

Figure 2. Typical TEM images of (a,b) Ag NPLs and (c,d) Ag@Au nanodisks. (e−g) EDS elemental mapping of Ag@Au nanodisks showing (e) Ag, (f) Au, and (f) overlay of Ag and Au elements.

To study the effect of the reaction solution pH on the galvanic reaction between Au^{3+} ions and Ag NPLs, we carried out a set of control experiments by changing the reaction conditions. (i) The synthesis was carried out at pH = 4, without introducing NaOH, keeping all other reaction conditions fixed. Surprisingly, the obtained products were bimetallic Ag@Au nanorings with well-defined interior gaps (Figure S2). EDS mapping and the line scanning analysis of the nanorings reveal their alloy (Ag@Au) nature (Figure S2d,e). As the reduction power of AA is low, at this condition, the rate of galvanic reaction becomes high ($R_{red} < R_{gal}$), resulting in the formation of hollow Ag@Au nanorings with well-defined pore diameter.[35] (ii) We increased the concentration of the HAuCl$_4$ precursor solution (2-fold higher than the concentration used for the fabrication of nanodisks), resulting in the formation of well-defined flower-like porous Ag@Au nanostructures (Figure S3). The formation of flower-like structures occurred because of the partial galvanic reaction between the Ag NPL seeds and Au^{3+} as well as the overgrowth of Au shells on the Ag NPLs. These results unambiguously confirm that the reaction pH and concentration of HAuCl$_4$ play crucial roles in controlling the reduction kinetics, which directly influence the shape of the final products.

In addition, previous studies have shown that the surfactant PVP can also favor in directing anisotropic growth.[53] In specific, PVP can prevent the oxidative etching events,[54] and the hydroxyl −OH groups present in the reaction mixture can act as mild reducing agents.[55] To validate the role played by PVP, we carried out two control experiments. First, the synthesis was carried out without the introduction of PVP, keeping all other conditions unchanged. As can be observed in Figure S4, disk-
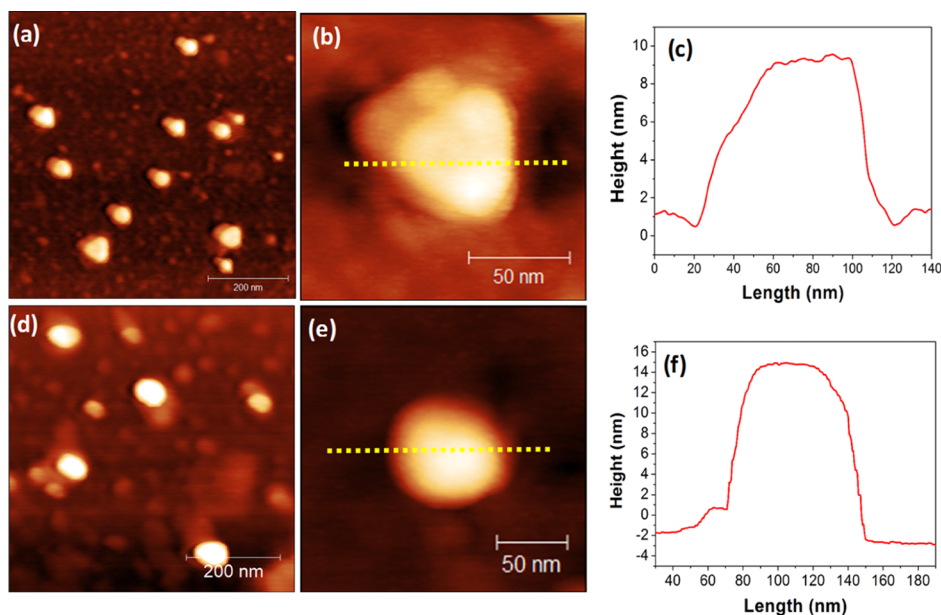
Figure 3. Typical AFM images of Ag NPLs (a,b) and Ag@Au nanodisks (d,e) supported over Si substrates. (c,f) Corresponding surface height profiles along the yellow dotted lines in (b,e). The increase of height for the Ag@Au nanodisks with respect to bare Ag NPLs indicates the formation of Au layer over them. The flat profile of the Ag@Au nanodisks (f) indicates their smooth/noncorrugated surface.
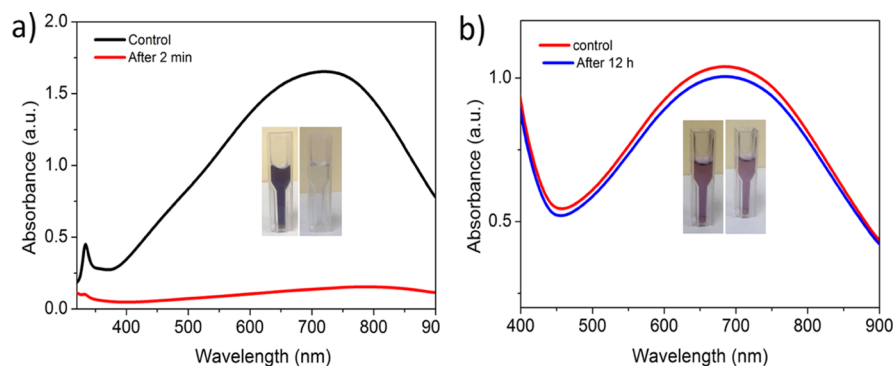

Figure 4. UV−vis absorption spectra of (a) bare Ag NPLs and (b) Ag@Au nanodisks before and after the addition of 2.3% aqueous H_2O_2. Insets show the corresponding photographic images before (left) and after (right) the addition of H_2O_2.

shaped nanostructures of different sizes were formed in the absence of PVP. The formation of few small Au NPs unevenly attached to disk-like nanostructures could also be observed (Figure S4). Second, PVP of the reaction mixture was replaced with another stabilizing agent CTAB of the same molar concentration. As can be seen in Figure S5, the addition of CTAB as the stabilizing agent leads to the formation of hexagonal Ag@Au NPs instead of Ag@Au nanodisks. The change in the morphology of the nanostructures can be ascribed to the selective binding of CTAB onto the (100) facet of Ag NPLs, which permits the oxidative etching to occur only at the corner sites of the Ag NPL seeds upon the introduction of Au^{3+} ion solution,[41] resulting in the formation of hexagonal Ag@Au nanostructures.

As the fabricated Ag@Au nanostructures contain silver (Ag), which is chemically unstable toward many chemical reactions, especially oxidation reactions,[56] we proceed to evaluate the chemical stability of the obtained Ag@Au nanodisks, monitoring their reaction with H_2O_2, a strong oxidant, through UV−vis spectroscopy. As can be seen in Figure 4a, the LSPR peak intensity of the original triangular Ag NPLs diminished within 2 min of the addition of about 0.2 mL aqueous H_2O_2 solution

(2.3%). By contrast, the Ag@Au nanodisks showed only a slight decrement in the SPR peak intensity even after 12 h of the addition of H_2O_2 solution (Figure 4b). The results clearly suggest a remarkable enhancement in the chemical stability of the Ag NPLs after their transformation to Ag@Au nanodisks. The improved chemical stability of the nanostructures is due to the formation of Au shell over the Ag NP surface.[29,50]

It is well-known that the bimetallic Ag@Au nanostructures exhibit size-dependent LSPR properties, which can be precisely adjusted from the visible to the NIR spectral range.[52] To monitor how a change in the diameter of Ag@Au nanodisks affects their LSPR, we fabricated Ag@Au nanodisks of different diameters by varying the amount of Ag NPL seeds in the reaction mixture. For this, we used 2, 5, 10, and 15 mL of Ag NPL seeds in the synthesis solution that yielded Ag@Au nanodisks of diameters 27, 33, 38, and 45 nm, respectively. The utilization of Ag NPLs in higher concentrations in the reaction mixture induced the formation of fewer Au sites at their edges. Consequently, there occurred a less oxidative etching reaction at the edges of the Ag NPLs and a higher overgrowth (of Au layer) onto their other faces, producing Ag@Au nanodisks of higher diameters. In fact, utilizing this procedure, Ag@Au nanodisks of
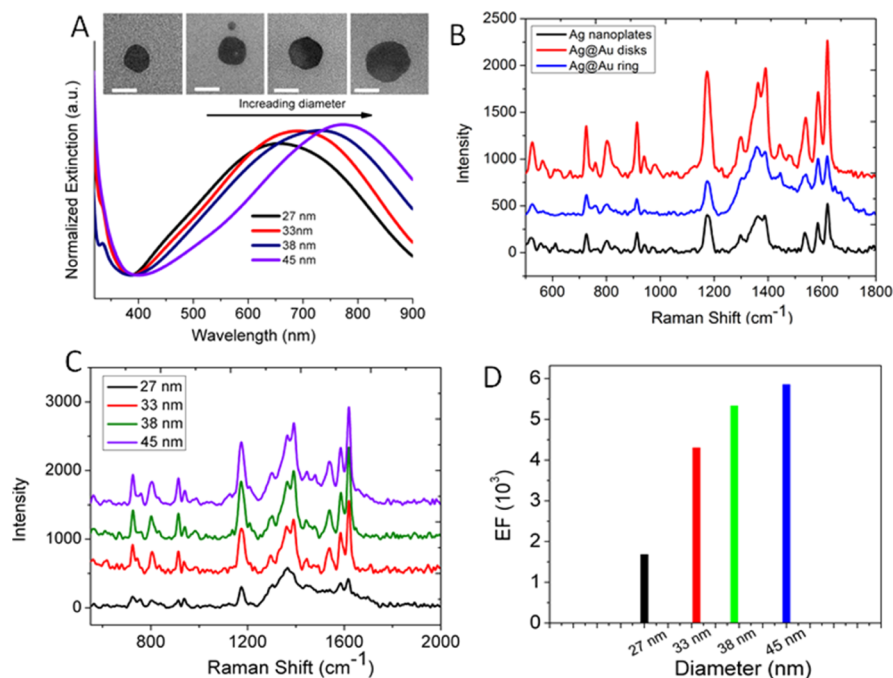
Figure 5. (A) Normalized UV−vis absorption spectra of the aqueous suspension of Ag@Au nanodisks of different diameters (27−45 nm). Insets show the TEM images of individual Au@Au nanodisks of increasing diameter. (B) Comparison of SERS spectra obtained from the aqueous solution of CV (10 μL of 10^{-6} M)-functionalized Ag NPLs, Ag@Au nanodisks, and Ag@Au nanorings, respectively. (C,D) SERS spectra of CV adsorbed on the Au@Au nanodisks of different diameters and corresponding EFs values.
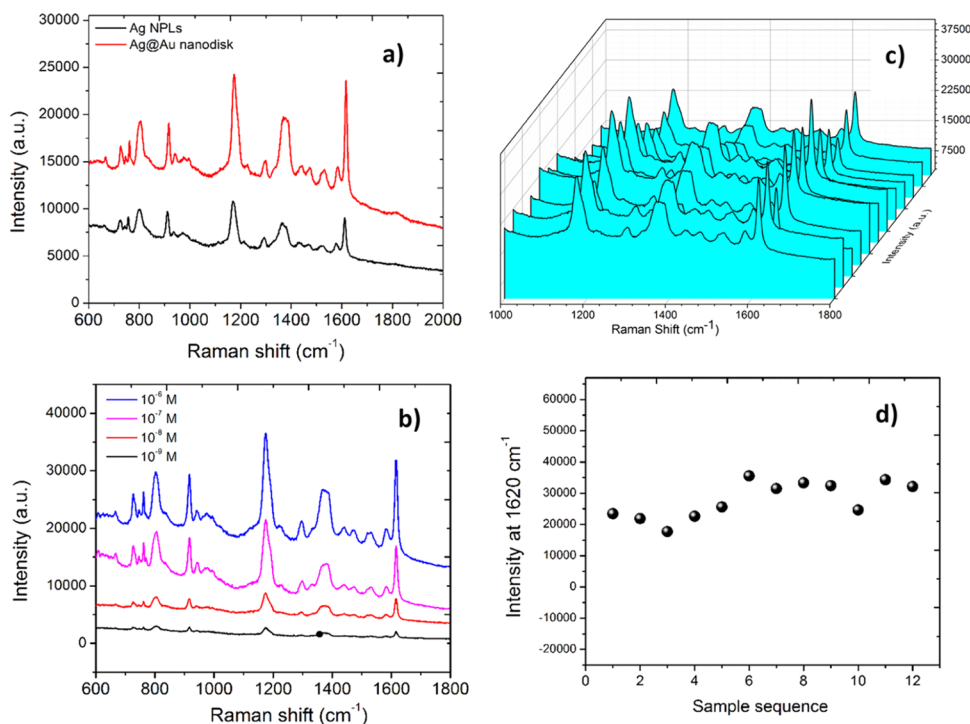

Figure 6. (a) Comparison of the SERS signals of bare AgNPLs and Ag@Au nanodisks deposited over Si substrates (CV, 1×10^{-6} M). (b) SERS spectra of Ag@Au nanodisks for different CV concentrations (from 10^{-6} to 10^{-9} M). (c) Reproducibility analysis of the SERS spectra of Ag@Au nanodisks (1×10^{-6} M CV) obtained from 12 randomly selected sites of the same substrate. (d) Corresponding peak intensity distribution at 1620 cm^{-1} for 12 sites of the SERS spectra.

different diameters could be fabricated with great control. The UV−vis absorption spectra of the Ag@Au nanostructures (Figure 5a) revealed that the characteristic LSPR peak at 656 nm for 27 nm nanodisks, which suffered red shifts to 689, 726, and 780 nm on increasing the diameter to 33, 38, and 45 nm,

respectively. The results are in accordance with the expected line, considering the variation of the effective dielectric constant of the bimetallic structures with the increase of the Au shell width.[57,58]

SERS Properties of Ag@Au Nanodisks. The SERS performance of Ag@Au nanodisks was studied using the aqueous solution-based SERS detection by incubating the plasmonic nanostructures in CV solutions and compared with the SERS performance of Ag@Au nanorings and Ag NPLs under the same conditions. The utilization of CV as a probe molecule in the present study is specifically because of its distinct Raman spectral features and the natural adsorption characteristic over the Au NP surface without chemical modifications.[59] Figure 5b compares the solution-phase SERS spectra of CV-adsorbed triangular Ag NPLs, Ag@Au nanorings, and Ag@Au nanodisks, respectively. As can be seen from Figure 5b, the obtained bimetallic Ag@Au nanodisks exhibit a significantly higher SERS signal intensity compared to the bare Ag NPLs and bimetallic Ag@Au nanorings.

The quantification of the SERS signal was performed by the estimation of SERS enhancement factor (EF) for the most prominent Raman peak at 1620 cm^{-1}, using the expression (eq 1)

$$\mathrm{EF} = \frac{I_{\mathrm{SERS}}}{N_{\mathrm{SERS}}} \bigg/ \frac{I_{\mathrm{Nor}}}{N_{\mathrm{Nor}}} \qquad (1)$$

where I_{SERS} and I_{Nor} are the SERS signal intensities of the sample and the normal Raman peak of CV at ~1620 cm^{-1}, and N_{SERS} and N_{Nor} are the corresponding values of the analyte probe molecules (CV) at the incident laser spot. We consider the adsorbed CV probe molecules distributed uniformly in aqueous solution; therefore, the values of N_{SERS} and N_{Nor} can be used with the CV concentrations such as 1.0×10^{-6} M (CV incubated with NPs) and 1.0×10^{-3} M (CV solution), respectively.

The signal EFs were estimated considering the intensity of the Raman peak appeared at 1620 cm^{-1} (Figure S6). The calculated EF for the Ag@Au nanodisks was 5.97×10^3, which is approximately 3- and 2.3-fold higher than the same for the Ag NPLs (2.0×10^3) and Ag@Au nanorings (2.55×10^3), respectively. In Figure 5c,d, we compare the SERS spectra of Ag@Au nanodisks of different diameters and their estimated signal EF values as a function of disk diameter. The results presented in Figure 5d demonstrate that the EF value increases with the diameter of the Ag@Au nanodisks. The Ag@Au nanodisks of higher diameters (45 nm) exhibit a higher signal EF compared to the Ag@Au nanodisks of lower diameters (Figure 5d). The observed results are in good agreement with the previous reports.[60,61]

It is largely believed that solid SERS substrates or films produce intense "hot spots", which improve significantly their SERS intensities.[62,63] Thus, we evaluated the substrate-based SERS performance by depositing the same amount of Ag NPL and Ag@Au nanodisk (45 nm diameter) samples over silicon (Si) substrates after drying the probe CV molecules (solution) over the samples prior to the SERS analysis (Figure 6a). As can be seen from Figure 6a, the substrate prepared with Ag@Au nanodisks exhibits much enhanced Raman signals in comparison to the Raman signal intensities obtained from their solution-casted counterpart. Apart from the effect of dispersion media (air in the first case and water in the second case),[64] the substrate-based assembly of plasmonic nanostructures seems to be of help in producing uniform and more intense "hot spots" which are responsible for the enhancement of Raman signal of the analytes. The Ag@Au nanodisks revealed highly intense Raman signals in comparison to the Ag NPLs. The EF values were calculated to be 0.18×10^5 and 0.47×10^5 for Ag NPLs and

Ag@Au nanodisks, respectively. In comparison to bare Ag NPLs, the Ag@Au nanodisks exhibited almost 2.5-fold higher EF values. The estimated SERS EF for Ag@Au nanodisk was slightly less compared to the previous reports of Ag@Au nanostructures, as shown in Table S1. The low EF estimated for our Ag@Au nanodisks might be due to their nonuniform distribution/assembly over the Si substrate, as the SERS substrates were prepared simply by drop-casing their colloidal solutions. On the other hand, as has been shown in the AFM results in Figure 2f, the obtained Ag@Au nanodisks have flat, noncorrugated surfaces, which generate plasmonic hot spots of relatively lower intensities.

To evaluate the SERS sensitivity of the Ag@Au nanodisks assembled over the Si substrate, we acquired the SERS spectra with different CV concentrations ranging from 1×10^{-6} to 1×10^{-9} M (Figure 6b). The SERS spectra for 1×10^{-6} M of CV revealed highly intense Raman peaks. However, their intensity decreased gradually on the reduction of CV concentration. To evaluate the SERS response of the fabricated Ag@Au nanodisks, the intensity of the 1620 cm^{-1} Raman dispersion peak of CV was recorded for different concentrations of the CV solution (Figure 6b). As can be observed in Figure S7 (Supporting Information), the intensity of this most intense Raman signal of CV varied linearly for the 10^{-6} to 10^{-9} M concentration range. In addition, as can be seen from Figure 6b, SERS signals are detectable even for the CV concentration of 10^{-9} M, suggesting that the resultant Ag@Au nanodisks are capable to detect CV molecules down to the 1×10^{-9} M concentration range. Notably, the observed sensitivity is comparable to the previous reports for bimetallic nanostructures (Table S1). The enhanced SERS efficiency of the Ag@Au nanodisks can be ascribed to two main plausible factors: (i) the LSPR peak of the Ag@Au disks at 780 nm is very near to the laser excitation wavelength used for recording the SERS spectra, which can be strongly coupled with the incident laser source, producing the resonance Raman effect.[65,66] (ii) The effective adsorption of CV molecules over the Ag@Au nanodisks and enhancement in the EM field between the nanogaps, which can serve as "hot spots" for a further increase in the SERS signal.[21] To demonstrate the reproducibility of the SERS substrates fabricated with Ag@Au nanodisks, the SERS spectra were measured at 12 different randomly selected sites of a substrate, for the CV concentration of 10^{-6} M. As can be observed in Figure 6c, the intensity of the SERS signal fluctuates by only about one order from place to place. The SERS reproducibility of the fabricated substrates was assessed by calculating the relative standard deviation (RSD) of the most dominant peak intensity at 1620 cm^{-1} (Figure 6d). The RSD value was obtained using the equation: RSD = SD/I_{m}, where SD is the standard deviation of the peak intensity and I_{m} is the average Raman peak intensities of the most dominant peaks.[67] The RSD of the 1620 cm^{-1} peak for 12 different sites was estimated to be 12.5%, indicating that the SERS substrates fabricated using Ag@Au nanodisks exhibit excellent reproducibility.

■ CONCLUSIONS

In summary, we present a simple, seed-mediated route for the fabrication of chemically stable bimetallic Ag@Au nanodisks with tunable LSPR response extending from the visible to the NIR spectral region. The high reaction pH and the tip-selective oxidative etching process utilized were found to be crucial for the suppression of the galvanic reaction, ultimately converting the triangular Ag NPLs into Ag@Au nanodisks. The obtained Ag@

Au nanodisks not only show enhanced chemical stability, but also excellent optical properties. By simply changing the amount of Ag NPL seed particles, Ag@Au nanodisks of diameters 27−45 nm, with tunable LSPR peak position from the visible to the NIR region could be fabricated. The as-prepared Ag@Au nanodisks exhibit highly enhanced SERS activity with the CV signal EF as high as 0.47×10^5. The SERS substrates prepared using the fabricated nanodisks can detect CV concentration down to 10^{-9} M. The synthesis approach utilized to prepare Ag@Au bimetallic nanostructures of high chemical stability and tunable plasmonic and SERS properties indicates that it is a promising technique for fabricating other type of core−shell bimetallic nanostructures for applications in plasmonics and biosensing.

■ EXPERIMENTAL DETAILS

Chemicals and Materials. Silver nitrate ($AgNO_3$, 99%), trisodium citrate ($Na_3C_6H_5O_7$, 99%), chloroauric acid ($HAuCl_4 \cdot 4H_2O$, 99.9%), sodium borohydride ($NaBH_4$, >98%), L-ascorbic acid (AA, 99%), PVP (MW of 55 K), CTAB (98%), hydrogen peroxide (H_2O_2, 30 wt % in H_2O), sodium hydroxide (NaOH, 98%), and CV (90%) were purchased from Sigma-Aldrich. All the chemicals were utilized as received and all the glasswares were washed thoroughly using deionized (DI) water prior to their use in experiments.

Synthesis of Ag NPL Seed NPs. The used process for the synthesis of Ag NPLs of ca. 25−35 nm edge lengths was similar to the process we reported earlier.[44] Briefly, 0.4 mL of 0.01 M aqueous $AgNO_3$ solution and 0.6 mL of 0.1 M trisodium citrate were mixed together, followed by the addition of DI water to make the final volume of the reaction solution of 40 mL. The mixture solution was magnetically stirred for 10 min, and then 0.4 mL of freshly prepared $NaBH_4$ solution (100 mM) was added. Subsequently, 0.1 mL of H_2O_2 was quickly injected to the previous solution. The color of the reaction mixture turned light yellow, yellow, red, green, and finally blue within 3−4 min. The final products (Ag NPLs) were collected by centrifugation at 12 000 rpm for about 30 min, followed by repeated washing in DI water.

Preparation of Bimetallic Ag@Au Nanodisks. The Ag@Au core−shell nanodisks were prepared by the seed-mediated growth process at room temperature using Ag NPLs as the template particles, PVP as the surfactant, and AA as the reducing agent. In a typical synthesis, 100 mg of AA and 66.6 mg of PVP were dissolved in 15 mL of DI water in a glass vial under magnetic stirring, after which 5 mL of the presynthesized aqueous suspension of Ag NPL seeds and 0.5 mL of 0.2 M aqueous NaOH solution were added into the reaction mixture sequentially. NaOH solution was added to increase the pH of the reaction mixture to 11.2. Then, the conformal deposition of Au and subsequent oxidative etching were performed by slow titration, adding 100 μL of 0.1 M aqueous $HAuCl_4$ precursor solution slowly (10 μL/min) by a syringe. The color of the solution mixture changed from dark blue to pink, indicating the formation of Ag@Au nanodisks. The product was collected by centrifugation at 12 000 rpm for 15 min and subsequent washing in DI water. The obtained product was redispersed in DI water. The formation of free AuNPs was avoided by optimizing the concentration of the Au precursor solution, injection rate, and the concentration of AA in the reaction mixture. The diameter of the Ag@Au nanodisks was controlled by simply varying the amount of Ag NPL seeds (5, 10, 15, and 20 mL) in the reaction mixture, keeping all other conditions fixed.

Materials Characterization. The UV−vis spectra of the samples were collected using an Agilent 8453 UV−vis spectrophotometer. The TEM images of the samples were collected in a JEOL JEM-1010 microscope operating at 80 kV. The EDS elemental mapping of the samples was carried out in a Hitachi SU 8020 microscope operating in STEM mode at an accelerating voltage of 20 kV. The samples for TEM and EDS mapping analysis were prepared by dispersing the colloidal nanostructures over carbon-coated Cu grids and subsequent drying at room temperature. AFM of the samples was performed in a Bruker (ScanAsyst-Air model) microscope operating in tapping mode. For AFM analysis, the colloidal nanostructures were deposited onto a Si substrate and dried overnight at ambient conditions. Room-temperature Raman and SERS spectra of the nanostructures were recorded in a Bruker (SENTERRA) Raman spectrometer equipped with an Ar-ion laser of 785 nm excitation wavelength (λ_{ex}).

Aqueous Solution-Based SERS Detection. The SERS spectra were obtained by using the same concentration of samples incubated in 25 μL of an aqueous solution of CV (10^{-6} M) for 2 h. The CV-adsorbed colloidal suspensions were then transferred to well-cleaned glass capillary tubes prior to SERS analysis. The Raman spectra of the solutions were collected using a 785 nm laser excitation source of 4.7 mW power with 4.0 μm beam diameter projected through a 50× objective lens.

Silicon Substrate-Based SERS Detection. The samples for substrate-based SERS were prepared by drying the same concentrations of the as-prepared AgNPL and Ag@Au nanodisk samples over clean silicon substrates (8 mm × 8 mm). In a typical procedure, 50 μL of each of the NP-containing suspensions (1 mg/mL) was deposited on Si substrates and then allowed to dry at room temperature. After this, 25 μL of an aqueous CV solution (10^{-6} M) was deposited over the sample and dried at room temperature. The Raman spectra were recorded using a 785 nm laser with the excitation source at room temperature. For all samples, the laser spot was fixed to 4 μM under a 50× objective lens; power density was 4.7 mW; and the signal acquisition time was set to be 3 s.

■ ASSOCIATED CONTENT

ⓢ Supporting Information

The Supporting Information is available free of charge on the ACS Publications website at DOI: 10.1021/acsomega.8b02333.

> TEM images and UV−vis absorption spectra of Ag NPLs, TEM images of different reaction products, SERS spectra of the samples, and details of the estimation of SERS EF values (PDF)

■ AUTHOR INFORMATION

Corresponding Author

*E-mail: sivakumar@ifuap.buap.mx.

ORCID ⓘ

Siva Kumar Krishnan: 0000-0002-9672-9335

Isaac. C. Sanchez: 0000-0003-4525-1199

Umapada Pal: 0000-0002-5665-106X

Notes

The authors declare no competing financial interest.

■ ACKNOWLEDGMENTS

■ REFERENCES

(1) Nasilowski, M.; Mahler, B.; Lhuillier, E.; Ithurria, S.; Dubertret, B. Two-Dimensional Colloidal Nanocrystals. *Chem. Rev.* **2016**, *116*, 10934−10982.

(2) Liu, S.; Tao, H.; Zeng, L.; Liu, Q.; Xu, Z.; Liu, Q.; Luo, J.-L. Shape-Dependent Electrocatalytic Reduction of CO_2 to CO on Triangular Silver Nanoplates. *J. Am. Chem. Soc.* **2017**, *139*, 2160−2163.

(3) Rycenga, M.; Cobley, C. M.; Zeng, J.; Li, W.; Moran, C. H.; Zhang, Q.; Qin, D.; Xia, Y. Controlling the Synthesis and Assembly of Silver Nanostructures for Plasmonic Applications. *Chem. Rev.* **2011**, *111*, 3669−3712.

(4) Tanaka, Y. Y.; Shimura, T. Tridirectional Polarization Routing of Light by a Single Triangular Plasmonic Nanoparticle. *Nano Lett.* **2017**, *17*, 3165−3170.

(5) Scarabelli, L.; Coronado-Puchau, M.; Giner-Casares, J. J.; Langer, J.; Liz-Marzán, L. M. Monodisperse Gold Nanotriangles: Size Control, Large-Scale Self-Assembly, and Performance in Surface-Enhanced Raman Scattering. *ACS Nano* **2014**, *8*, 5833−5842.

(6) Charles, D. E.; Aherne, D.; Gara, M.; Ledwith, D. M.; Gun'ko, Y. K.; Kelly, J. M.; Blau, W. J.; Brennan-Fournet, M. E. Versatile Solution Phase Triangular Silver Nanoplates for Highly Sensitive Plasmon Resonance Sensing. *ACS Nano* **2010**, *4*, 55−64.

(7) Giner-Casares, J. J.; Liz-Marzán, L. M. Plasmonic nanoparticles in 2D for biological applications: Toward active multipurpose platforms. *Nano Today* **2014**, *9*, 365−377.

(8) Kneipp, J.; Kneipp, H.; Kneipp, K. SERS-a Single-Molecule and Nanoscale Tool for Bioanalytics. *Chem. Soc. Rev.* **2008**, *37*, 1052−1060.

(9) Wang, Z.; Zong, S.; Wu, L.; Zhu, D.; Cui, Y. SERS-Activated Platforms for Immunoassay: Probes, Encoding Methods, and Applications. *Chem. Rev.* **2017**, *117*, 7910−7963.

(10) Moskovits, M. Surface-Enhanced Spectroscopy. *Rev. Mod. Phys.* **1985**, *57*, 783−826.

(11) Li, C.-Y.; Meng, M.; Huang, S.-C.; Li, L.; Huang, S.-R.; Chen, S.; Meng, L.-Y.; Panneerselvam, R.; Zhang, S.-J.; Ren, B.; Yang, Z.-L.; Li, J.-F.; Tian, Z.-Q. "Smart" Ag Nanostructures for Plasmon-Enhanced Spectroscopies. *J. Am. Chem. Soc.* **2015**, *137*, 13784−13787.

(12) Mulvihill, M. J.; Ling, X. Y.; Henzie, J.; Yang, P. Anisotropic Etching of Silver Nanoparticles for Plasmonic Structures Capable of Single-Particle SERS. *J. Am. Chem. Soc.* **2010**, *132*, 268−274.

(13) Kuttner, C.; Mayer, M.; Dulle, M.; Moscoso, A.; López-Romero, J. M.; Förster, S.; Fery, A.; Pérez-Juste, J.; Contreras-Cáceres, R. Seeded Growth Synthesis of Gold Nanotriangles: Size Control, SAXS Analysis, and SERS Performance. *ACS Appl. Mater. Interfaces* **2018**, *10*, 11152−11163.

(14) Hanske, C.; González-Rubio, G.; Hamon, C.; Formentín, P.; Modin, E.; Chuvilin, A.; Guerrero-Martínez, A.; Marsal, L. F.; Liz-Marzán, L. M. Large-Scale Plasmonic Pyramidal Supercrystals via Templated Self-Assembly of Monodisperse Gold Nanospheres. *J. Phys. Chem. C* **2017**, *121*, 10899−10906.

(15) Kim, J.; Song, X.; Ji, F.; Luo, B.; Ice, N. F.; Liu, Q.; Zhang, Q.; Chen, Q. Polymorphic Assembly from Beveled Gold Triangular Nanoprisms. *Nano Lett.* **2017**, *17*, 3270−3275.

(16) Li, J.-F.; Zhang, Y.-J.; Rudnev, A. V.; Anema, J. R.; Li, S.-B.; Hong, W.-J.; Rajapandiyan, P.; Lipkowski, J.; Wandlowski, T.; Tian, Z.-Q. Electrochemical Shell-Isolated Nanoparticle-Enhanced Raman Spectroscopy: Correlating Structural Information and Adsorption Processes of Pyridine at the Au(hkl) Single Crystal/solution Interface. *J. Am. Chem. Soc.* **2015**, *137*, 2400−2408.

(17) Kelly, K. L.; Coronado, E.; Zhao, L. L.; Schatz, G. C. The Optical Properties of Metal Nanoparticles: The Influence of Size, Shape, and Dielectric Environment. *J. Phys. Chem. B* **2003**, *107*, 668−677.

(18) Zhang, Q.; Hu, Y.; Guo, S.; Goebl, J.; Yin, Y. Seeded Growth of Uniform Ag Nanoplates with High Aspect Ratio and Widely Tunable Surface Plasmon Bands. *Nano Lett.* **2010**, *10*, 5037−5042.

(19) Pastoriza-Santos, I.; Liz-Marzán, L. M. Colloidal silver nanoplates. State of the art and future challenges. *J. Mater. Chem.* **2008**, *18*, 1724−1737.

(20) Li, J.-F.; Zhang, Y.-J.; Ding, S.-Y.; Panneerselvam, R.; Tian, Z.-Q. Core-Shell Nanoparticle-Enhanced Raman Spectroscopy. *Chem. Rev.* **2017**, *117*, 5002−5069.

(21) Liu, K.; Bai, Y.; Zhang, L.; Yang, Z.; Fan, Q.; Zheng, H.; Yin, Y.; Gao, C. Porous Au-Ag Nanospheres with High-Density and Highly Accessible Hotspots for SERS Analysis. *Nano Lett.* **2016**, *16*, 3675−3681.

(22) Rao, V. K.; Radhakrishnan, T. P. Tuning the SERS Response with Ag-Au Nanoparticle-Embedded Polymer Thin Film Substrates. *ACS Appl. Mater. Interfaces* **2015**, *7*, 12767−12773.

(23) Fan, M.; Lai, F.-J.; Chou, H.-L.; Lu, W.-T.; Hwang, B.-J.; Brolo, A. G. Surface-Enhanced Raman Scattering (SERS) from Au:Ag Bimetallic Nanoparticles: The Effect of the Molecular Probe. *Chem. Sci.* **2013**, *4*, 509−515.

(24) Yin, H. J.; Chen, Z. Y.; Zhao, Y. M.; Lv, M. Y.; Shi, C. A.; Wu, Z. L.; Zhang, X.; Liu, L.; Wang, M. L.; Xu, H. J. Ag@Au Core-Shell Dendrites: A Stable, Reusable and Sensitive Surface Enhanced Raman Scattering Substrate. *Sci. Rep.* **2015**, *5*, 14502.

(25) Yin, Z.; Wang, Y.; Song, C.; Zheng, L.; Ma, N.; Liu, X.; Li, S.; Lin, L.; Li, M.; Xu, Y.; Li, W.; Hu, G.; Fang, Z.; Ma, D. Hybrid Au-Ag Nanostructures for Enhanced Plasmon-Driven Catalytic Selective Hydrogenation through Visible Light Irradiation and Surface-Enhanced Raman Scattering. *J. Am. Chem. Soc.* **2018**, *140*, 864−867.

(26) Dai, L.; Song, L.; Huang, Y.; Zhang, L.; Lu, X.; Zhang, J.; Chen, T. Bimetallic Au/Ag Core-Shell Superstructures with Tunable Surface Plasmon Resonance in the Near-Infrared Region and High Performance Surface-Enhanced Raman Scattering. *Langmuir* **2017**, *33*, 5378−5384.

(27) Zhang, J.; Winget, S. A.; Wu, Y.; Su, D.; Sun, X.; Xie, Z.-X.; Qin, D. Ag@Au Concave Cuboctahedra: A Unique Probe for Monitoring Au-Catalyzed Reduction and Oxidation Reactions by Surface-Enhanced Raman Spectroscopy. *ACS Nano* **2016**, *10*, 2607−2616.

(28) Yang, Y.; Liu, J.; Fu, Z.-W.; Qin, D. Galvanic Replacement-Free Deposition of Au on Ag for Core-Shell Nanocubes with Enhanced Chemical Stability and SERS Activity. *J. Am. Chem. Soc.* **2014**, *136*, 8153−8156.

(29) Liu, H.; Liu, T.; Zhang, L.; Han, L.; Gao, C.; Yin, Y. Etching-Free Epitaxial Growth of Gold on Silver Nanostructures for High Chemical Stability and Plasmonic Activity. *Adv. Funct. Mater.* **2015**, *25*, 5435−5443.

(30) Cathcart, N.; Chen, J. I. L.; Kitaev, V. LSPR Tuning from 470 to 800 nm and Improved Stability of Au-Ag Nanoparticles Formed by Gold Deposition and Rebuilding in the Presence of Poly-(styrenesulfonate). *Langmuir* **2018**, *34*, 612−621.

(31) Weiner, R. G.; Kunz, M. R.; Skrabalak, S. E. Seeding a New Kind of Garden: Synthesis of Architecturally Defined Multimetallic Nanostructures by Seed-Mediated Co-Reduction. *Acc. Chem. Res.* **2015**, *48*, 2688−2695.

(32) Yan, Y.; Shan, H.; Li, G.; Xiao, F.; Jiang, Y.; Yan, Y.; Jin, C.; Zhang, H.; Wu, J.; Yang, D. Epitaxial Growth of Multimetallic Pd@PtM (M = Ni, Rh, Ru) Core-Shell Nanoplates Realized by in Situ-Produced CO from Interfacial Catalytic Reactions. *Nano Lett.* **2016**, *16*, 7999−8004.

(33) Bian, T.; Zhang, H.; Jiang, Y.; Jin, C.; Wu, J.; Yang, H.; Yang, D. Epitaxial Growth of Twinned Au-Pt Core-Shell Star-Shaped Decahedra as Highly Durable Electrocatalysts. *Nano Lett.* **2015**, *15*, 7808−7815.

(34) Hsu, S.-C.; Chuang, Y.-C.; Sneed, B. T.; Cullen, D. A.; Chiu, T.-W.; Kuo, C.-H. Turning the Halide Switch in the Synthesis of Au-Pd Alloy and Core-Shell Nanoicosahedra with Terraced Shells: Performance in Electrochemical and Plasmon-Enhanced Catalysis. *Nano Lett.* **2016**, *16*, 5514−5520.

(35) Lu, X.; Tuan, H.-Y.; Chen, J.; Li, Z.-Y.; Korgel, B. A.; Xia, Y. Mechanistic Studies on the Galvanic Replacement Reaction between Multiply Twinned Particles of Ag and HAuCl4 in an Organic Medium. *J. Am. Chem. Soc.* **2007**, *129*, 1733−1742.

(36) Me, G. S.; Cao, Y. C.; Jin, R.; Mirkin, C. A. Triangular Nanoframes Made of Gold and Silver. *Nano Lett.* **2003**, *3*, 519−522.

(37) Moreau, L. M.; Schurman, C. A.; Kewalramani, S.; Shahjamali, M. M.; Mirkin, C. A.; Bedzyk, M. J. How Ag Nanospheres Are Transformed into AgAu Nanocages. *J. Am. Chem. Soc.* **2017**, *139*, 12291−12298.

(38) Shahjamali, M. M.; Bosman, M.; Cao, S.; Huang, X.; Saadat, S.; Martinsson, E.; Aili, D.; Tay, Y. Y.; Liedberg, B.; Loo, S. C. J.; Zhang, H.; Boey, F.; Xue, C. Gold Coating of Silver Nanoprisms. *Adv. Funct. Mater.* **2012**, *22*, 849−854.

(39) Gao, C.; Lu, Z.; Liu, Y.; Zhang, Q.; Chi, M.; Cheng, Q.; Yin, Y. Highly Stable Silver Nanoplates for Surface Plasmon Resonance Biosensing. *Angew. Chem. Int. Ed.* **2012**, *51*, 5629−5633.

(40) Murshid, N.; Gourevich, I.; Coombs, N.; Kitaev, V. Gold Plating of Silver Nanoparticles for Superior Stability and Preserved Plasmonic and Sensing Properties. *Chem. Commun.* **2013**, *49*, 11355−11357.

(41) O'Brien, M. N.; Jones, M. R.; Brown, K. A.; Mirkin, C. A. Universal Noble Metal Nanoparticle Seeds Realized Through Iterative Reductive Growth and Oxidative Dissolution Reactions. *J. Am. Chem. Soc.* **2014**, *136*, 7603−7606.

(42) Hong, S.; Shuford, K. L.; Park, S. Shape Transformation of Gold Nanoplates and Their Surface Plasmon Characterization: Triangular to Hexagonal Nanoplates. *Chem. Mater.* **2011**, *23*, 2011−2013.

(43) Lin, X.; Lin, S.; Liu, Y.; Gao, M.; Zhao, H.; Liu, B.; Hasi, W.; Wang, L. Facile Synthesis of Monodisperse Silver Nanospheres in Aqueous Solution via Seed-Mediated Growth Coupled with Oxidative Etching. *Langmuir* **2018**, *34*, 6077−6084.

(44) Kumar-Krishnan, S.; Estevez-González, M.; Pérez, R.; Esparza, R.; Meyyappan, M. A general seed-mediated approach to the synthesis of AgM (M = Au, Pt, and Pd) core-shell nanoplates and their SERS properties. *RSC Adv.* **2017**, *7*, 27170−27176.

(45) Aslam, U.; Linic, S. Addressing Challenges and Scalability in the Synthesis of Thin Uniform Metal Shells on Large Metal Nanoparticle Cores: Case Study of Ag-Pt Core-Shell Nanocubes. *ACS Appl. Mater. Interfaces* **2017**, *9*, 43127−43132.

(46) Ahn, J.; Wang, D.; Ding, Y.; Zhang, J.; Qin, D. Site-Selective Carving and Co-Deposition: Transformation of Ag Nanocubes into Concave Nanocrystals Encased by Au-Ag Alloy Frames. *ACS Nano* **2018**, *12*, 298−307.

(47) Daniel, J. R.; McCarthy, L. A.; Yazdi, S.; Chagnot, M.; Ringe, E.; Boudreau, D. Gold Speciation and Co-Reduction Control the Morphology of AgAu Nanoshells in Formaldehyde-Assisted Galvanic Replacement. *J. Phys. Chem. C* **2018**, *122*, 18168−18176.

(48) An, J.; Tang, B.; Zheng, X.; Zhou, J.; Dong, F.; Xu, S.; Wang, Y.; Zhao, B.; Xu, W. Sculpturing Effect of Chloride Ions in Shape Transformation from Triangular to Discal Silver Nanoplates. *J. Phys. Chem. C* **2008**, *112*, 15176−15182.

(49) Xu, S.; Tang, B.; Zheng, X.; Zhou, J.; An, J.; Ning, X.; Xu, W. The Facet Selectivity of Inorganic Ions on Silver Nanocrystals in Etching Reactions. *Nanotechnology* **2009**, *20*, 415601.

(50) Yang, M.; Hood, Z. D.; Yang, X.; Chi, M.; Xia, Y. Facile Synthesis of Ag@Au Core-Sheath Nanowires with Greatly Improved Stability against Oxidation. *Chem. Commun.* **2017**, *53*, 1965−1968.

(51) Hong, S.; Acapulco, J. A. I.; Jang, H. Y.; Park, S. Au Nanodisk-Core Multishell Nanoparticles: Synthetic Method for Controlling Number of Shells and Intershell Distance. *Chem. Mater.* **2014**, *26*, 3618−3623.

(52) O'Brien, M. N.; Jones, M. R.; Kohlstedt, K. L.; Schatz, G. C.; Mirkin, C. A. Uniform Circular Disks With Synthetically Tailorable Diameters: Two-Dimensional Nanoparticles for Plasmonics. *Nano Lett.* **2015**, *15*, 1012−1017.

(53) Zhai, Y.; DuChene, J. S.; Wang, Y.-C.; Qiu, J.; Johnston-Peck, A. C.; You, B.; Guo, W.; DiCiaccio, B.; Qian, K.; Zhao, E. W.; Ooi, F.; Hu, D.; Su, D.; Stach, E. A.; Zhu, Z.; Wei, W. D. Polyvinylpyrrolidone-Induced Anisotropic Growth of Gold Nanoprisms in Plasmon-Driven Synthesis. *Nat. Mater.* **2016**, *1−8*, 889−895.

(54) Sun, H.; He, J.; Wang, J.; Zhang, S.-Y.; Liu, C.; Sritharan, T.; Mhaisalkar, S.; Han, M.-Y.; Wang, D.; Chen, H. Investigating the Multiple Roles of Polyvinylpyrrolidone for a General Methodology of Oxide Encapsulation. *J. Am. Chem. Soc.* **2013**, *135*, 9099−9110.

(55) Yin, Y.; Alivisatos, A. P. Colloidal Nanocrystal Synthesis and the Organic-Inorganic Interface. *Nature* **2005**, *437*, 664−670.

(56) Pech-Pech, I. E.; Gervasio, D. F.; Pérez-Robles, J. F. Nanoparticles of Ag with a Pt and Pd Rich Surface Supported on Carbon as a New Catalyst for the Oxygen Electroreduction Reaction (ORR) in Acid Electrolytes: Part 2. *J. Power Sources* **2015**, *276*, 374−381.

(57) Coronado, E. A.; Schatz, G. C. Surface Plasmon Broadening for Arbitrary Shape Nanoparticles: A Geometrical Probability Approach. *J. Chem. Phys.* **2003**, *119*, 3926−3934.

(58) Wang, X.; Zhang, Z.; Hartland, G. V. Electronic Dephasing in Bimetallic Gold−Silver Nanoparticles Examined by Single Particle Spectroscopy. *J. Phys. Chem. B* **2005**, *109*, 20324−20330.

(59) Zhang, L.-F.; Zhong, S.-L.; Xu, A.-W. Highly Branched Concave Au/Pd Bimetallic Nanocrystals with Superior Electrocatalytic Activity and Highly Efficient SERS Enhancement. *Angew. Chem. Int. Ed.* **2013**, *52*, 645−649.

(60) Ross, M. B.; Ashley, M. J.; Schmucker, A. L.; Singamaneni, S.; Naik, R. R.; Schatz, G. C.; Mirkin, C. A. Structure-Function Relationships for Surface-Enhanced Raman Spectroscopy-Active Plasmonic Paper. *J. Phys. Chem. C* **2016**, *120*, 20789−20797.

(61) Meng, M.; Fang, Z.; Zhang, C.; Su, H.; He, R.; Zhang, R.; Li, H.; Li, Z.-Y.; Wu, X.; Ma, C.; Zeng, J. Integration of Kinetic Control and Lattice Mismatch To Synthesize Pd@AuCu Core-Shell Planar Tetrapods with Size-Dependent Optical Properties. *Nano Lett.* **2016**, *16*, 3036−3041.

(62) Niu, W.; Chua, Y. A. A.; Zhang, W.; Huang, H.; Lu, X. Highly Symmetric Gold Nanostars: Crystallographic Control and Surface-Enhanced Raman Scattering Property. *J. Am. Chem. Soc.* **2015**, *137*, 10460−10463.

(63) Shin, H.-H.; Yeon, G. J.; Choi, H.-K.; Park, S.-M.; Lee, K. S.; Kim, Z. H. Frequency-Domain Proof of the Existence of Atomic-Scale SERS Hot-Spots. *Nano Lett.* **2018**, *18*, 262−271.

(64) Montaño-Priede, J. L.; Peña-Rodríguez, O.; Pal, U. Near-Electric-Field Tuned Plasmonic Au@SiO$_2$ and Ag@SiO$_2$ Nanoparticles for Efficient Utilization in Luminescence Enhancement and Surface-Enhanced Spectroscopy. *J. Phys. Chem. C* **2017**, *121*, 23062−23071.

(65) Cha, S. K.; Mun, J. H.; Chang, T.; Kim, S. Y.; Kim, J. Y.; Jin, H. M.; Lee, J. Y.; Shin, J.; Kim, K. H.; Kim, S. O. Au-Ag Core-Shell Nanoparticle Array by Block Copolymer Lithography for Synergistic Broadband Plasmonic Properties. *ACS Nano* **2015**, *9*, 5536−5543.

(66) Li, M.; Kang, J. W.; Dasari, R. R.; Barman, I. Shedding Light on the Extinction-Enhancement Duality in Gold Nanostar-Enhanced Raman Spectroscopy. *Angew. Chem. Int. Ed.* **2014**, *53*, 14115−14119.

(67) Xin, W.; Yang, J.-M.; Li, C.; Goorsky, M. S.; Carlson, L.; De Rosa, I. M. Novel Strategy for One-Pot Synthesis of Gold Nanoplates on Carbon Nanotube Sheet As an Effective Flexible SERS Substrate. *ACS Appl. Mater. Interfaces* **2017**, *9*, 6246−6254.